Relaxation dynamics in dense binary colloidal mixtures: Brownian dynamics simulations

Subrata Sanyal*
Department of Chemical Engineering, University of California at Santa Barbara, Santa Barbara, California 93106-5080

Ajay K. Sood†
Department of Physics, Indian Institute of Science, Bangalore 560 012, India
(Received 1 April 1996; revised manuscript received 18 August 1997)

Brownian dynamics simulations have been carried out on a binary colloidal mixture of particles of two different diameters interacting via a Derjaguin-Landau-Verway-Overbeek potential. As the screening length is increased a transition from liquid to crystal (at a volume fraction $\phi=0.2$) or a glassy state (at $\phi=0.3$) is observed. Below a certain effective temperature $T^{\star}$, the temporal evolution of the mean-squared displacements shows a marked subdiffusive behavior at intermediate and long times. The supercooled liquid with $\phi=0.3$ shows a staircase profile indicating strongly cooperative jump motion which is corroborated by the behavior of van Hove self-correlation functions and the non-Gaussian parameter. The van Hove distinct correlation function, in the β relaxation regime, shows a factorization property in accordance with the mode-coupling theory predictions. The most interesting result is the observation of cooperative hop and subsequent hop-back motion at temperatures close to the glass transition. [S1063-651X(98)10401-4]

PACS number(s): 82.70.Dd, 61.20.Ja, 05.40.+j, 64.70.Dv

I. INTRODUCTION

Charge-stabilized aqueous colloidal suspensions of polystyrene particles (polyballs) and sterically stabilized nearly hard-sphere colloids of polymethyl methacrylate (PMMA) particles are considered to be model condensed matter systems to study a rich variety of cooperative behavior in equilibrium and nonequilibrium conditions because their interparticle interactions can be easily controlled. Liquid, crystalline, and even glassy states are seen in these systems [1] under suitable experimental conditions. One-component polyball systems show either a body-centered cubic (bcc) phase at low volume fractions ϕ or a face-centered cubic phase at high ϕ. The glassy state in these systems at $\phi \sim 0.2$ was revealed by small-angle neutron scattering measurements [2] of structure factors. The freezing of monodisperse PMMA suspensions from a liquid to an equilibrium crystalline phase or a metastable glassy state has been studied extensively [3] as a function of ϕ [4]. In binary colloids, the structural behavior is much richer. Several compound crystalline structures like AB_2, AB_4, and AB_{13} have been identified in concentrated polyball suspensions [5] as well as in PMMA colloids [6]. Existence of glassy states in binary mixtures of charged colloids has been inferred from the measurements of shear modulus [7] and static structure factors by light scattering [8], diffusing wave spectroscopy experiments [9], and computer simulations [10].

The use of mode-coupling theories (MCT) has achieved a significant advancement in understanding the microscopic dynamical behavior of supercooled liquids near ''glass transition'' (GT). Its idealized version [11], which was shown to hold good for colloidal suspensions too [12], explicitly incorporates the delayed nonlinear coupling between density fluctuations and projects the following picture for particle dynamics in dense liquids. The motion of a particle is continuously hindered by the cages formed by its surrounding particles. The fact that a caged particle can be considered a member of another neighboring cage results in a cooperative movement of a large number of particles. With cooling (or increasing density ϕ), this coupling and hence the structural relaxation time increases and ultimately diverges at a critical temperature T_c (or a critical density ϕ_c). The static properties vary smoothly across T_c (or ϕ_c) but the dynamic properties change abruptly from an ergodic (fluidlike) to a nonergodic (solidlike) behavior corresponding to a complete arrest of concentration fluctuations of all length scales. Near T_c (or ϕ_c), the idealized MCT predicts the onset of two distinct relaxation processes beyond microscopic relaxation time τ_0, namely, a long-time α relaxation and an intermediate-time β relaxation. Although β relaxation persists in the glassy states, α relaxation freezes out, giving rise to a sharp liquid-glass transition. This sort of a sharp transition is never seen in experiments and simulations because of the presence of phonon activated transport (hopping) processes which restore α relaxation in glass and hence make the crossover from liquid to glass smooth. An extended version of MCT [13] incorporates the activated motion and the light scattering data [14] for both molecular glass Salol and the ionic glass $Ca_{0.4}K_{0.6}(NO_3)_{1.4}$ are seen to agree well with its predictions. However, the dielectric susceptibility measurements [15] of Salol do not match well with the above.

Computer simulations are ideal to study the static and dynamic properties of model systems. The molecular dynamics (MD) simulations have been extensively used to study the dynamics of binary supercooled liquids as it approaches glass transition, for example, for particles interacting via Lennard-Jones (LJ) [16], purely repulsive r^{-12} [17], and

*Author to whom correspondence should be addressed. Electronic address: subrata@navier.chemengr.ucsb.edu

†Also at Jawaharlal Nehru Center for Advanced Scientific Research, Jakkur Campus, P.O.: Jakkur, Bangalore 560 064, Karnataka, India. Electronic address: asood@physics.iisc.ernet.in

 © 1998 The American Physical Society

size-corrected Yukawa potential [18]. Liquid, crystalline, and glassy states were observed in the MD simulation of binary polyball mixtures [18]. The fluid molecules, being much smaller than the polyballs, provide a uniform viscous medium in which the motion of the polyballs is overdamped. Thus the simulation technique appropriate to polyball suspensions is Brownian dynamics (BD) [19]. The influence of the Newtonian (MD) and Brownian (BD) dynamics on the dynamical correlations for liquid to GT in charge-polydisperse colloids has been investigated in a previous simulation study [10]. It was shown that though the long-time relaxation scenarios of density correlation functions in both the cases are similar, they differ in the short and intermediate times.

The aim of the present paper is to understand the slow dynamics of a charge-stabilized dense colloidal liquid as it is ''cooled'' (defined later) and the relevance of activated motion at effective low temperatures. To this end, we report our BD simulation results on the dynamical parameters as a binary dense liquid is cooled by reducing the impurity ion concentration n_i in steps to a crystal at $\phi=0.2$ or a metastable glass at $\phi=0.3$. The dynamical quantities that we have probed are the mean-squared displacements (MSD's), time-dependent diffusion constants $D(t)$, self part $G_\alpha^s(r,t)$, and distinct part $G_\alpha^d(r,t)$ of the van Hove correlation function and non-Gaussian parameter $a_\alpha(t)$. Detailed studies on the static parameters [20] and the calculations of translational and bond-orientational correlation functions [21] that supplement our conclusions are reported elsewhere. In order to look carefully into the presence of activated hops and cooperativeness in particle motion, we have also probed the particle displacements directly. The paper is set out as follows. In Sec. II we describe the model and details of the simulation. Section III is devoted to the results and finally, Sec. IV contains the summary of our findings and conclusions.

II. MODEL AND DETAILS OF SIMULATION

Since the model and our simulation procedure have already been detailed elsewhere [20], we will briefly touch upon the main points here. We consider a binary polyball mixture of $N_1=N_2=216$ particles with the lighter particles having a radius $a_1=545$ Å, a valence $Z_1=300$ and the heavier particles having $a_2=1100$ Å and $Z_2=600$. It is identical to the experimental system of Lindsay and Chaikin [7] as well as the one used in the MD simulation of Rosenberg *et al.* [18]. The interparticle interaction is modeled via a purely repulsive, size-corrected Derjaguin-Landau-Verway-Overbeek (DLVO) potential [1]

$$U_{ij}(r)=\frac{Z_iZ_je^2}{\epsilon}\left(\frac{e^{\kappa a_i}}{1+\kappa a_i}\right)\left(\frac{e^{\kappa a_j}}{1+\kappa a_j}\right)\frac{e^{-\kappa r}}{r}, \tag{1}$$

where ϵ is the dielectric constant of water (equal to 78) at temperature T (equal to 298 K). For a binary suspension, the inverse Debye-Hückel screening length κ is given by

$$\kappa^2=\frac{4\pi e^2}{\epsilon k_BT}\left(n_p\overline{Z}+\sum_i n_iz_i^2\right), \tag{2}$$

where n_p and n_i are the total number densities of particles and monovalent impurity ions (i.e., $z_i=1$), respectively. Here, $\overline{Z}=xZ_1+(1-x)Z_2$, with the composition variable $x=N_1/N$ $(=0.5)$. The system can be suitably characterized by its total volume fraction

$$\phi=\frac{4}{3}\pi n_p[xa_1^3+(1-x)a_2^3] \tag{3}$$

and reduced temperature $T^\star$, given by

$$\frac{1}{T^\star}=\frac{U_0}{k_BT}=\frac{(\overline{Ze})^2}{\epsilon k_BT}\left(\frac{e^{\kappa\overline{a}}}{1+\kappa\overline{a}}\right)^2\frac{e^{-\kappa a_s}}{a_s}, \tag{4}$$

where U_0 is the energy scale. Here $\overline{a}$ is the mean radius and $a_s=n_p^{-1/3}$ is the average interparticle separation. The particle positions are updated at every time step δt according to the finite-difference BD algorithm due to Ermak and Yeh [19]. The random part and the inaccuracies involved in the calculation of the systematic part of force in the algorithm may lead to spurious movements of the center of mass of the system as a whole. This is corrected by holding the center of mass fixed at each position updating. The cutoff distance r_c for the potential is chosen to be equal to $2a_s$ or $6\kappa^{-1}$, whichever is greater, to ensure that $U_{ij}(r_c)\sim 0.001k_BT$. We have used the cubic periodic boundary conditions and its natural consequence—-the minimum image convention [22]—to minimize the surface effects.

As shown in Table I, at each ϕ, an initial bcc lattice is melted into a liquid with a high impurity concentration $n_i=5n_p\overline{Z}$ and this liquid is then sequentially ''cooled'' in 11 more steps with n_i at every step being half of the previous one, except for the last step where $n_i=0$. The runs in the sequence are named as $X0, Xa, Xb, \ldots, Xk$ for $\phi=0.2$ and $G0, Ga, Gb, \ldots, Gk$ for $\phi=0.3$. With this method of cooling, called ''slow quench,'' the effective temperature $T^\star$ of the system is brought down from ~ 1 to ~ 0.03. At each $T^\star$, monitoring total and partial pair distribution functions (PDF's) over the entire equilibration run of $N_{\rm eq}$ time steps $(\sim 2\times 10^6\,\delta t)$ together with a steady value (rms deviation being less than or equal to 0.15%) of the internal energy per particle $E=(1/Nk_BT)\Sigma_{j\neq i}U_{ij}(r)$ ensure a proper equilibration. Next $N_{\rm PR}$ $(\sim 3\times 10^6\,\delta t)$ steps (production run) (see Table I) are used for evaluating the static [20] and dynamic quantities reported here, as well as the density and the bond-orientational correlation functions [21].

The characteristics of the BD runs for $\phi=0.2$ and 0.3 are given in Table I. We note that runs Xl and Xm are independent runs and are not similar to the other slow-quench runs. If the particles are put on a bcc lattice irrespective of their species and then simulated with parameters the same as run Xk (i.e., $\phi=0.2$ and $n_i=0$) the final state Xl is a bcc with improper sublattice ordering. By contrast, if an initial bcc composed of two interpenetrating simple cubic sublattices made of either kind of particles is simulated with parameters as above, the final state Xm is a substitutionally ordered bcc. By comparing the internal energy E and the PDF, the position and type of the immediate eight neighbors of each particle and translational and bond-orientational orders [21] of runs Xk, Xl, and Xm, we conclude [23] that the resulting

TABLE I. Cooling history of different runs. The parameters are explained in the text.

Run	N_{eq}	N_{PR}	$n_i/(n_p\overline{Z})$	$T^\star$	κa_s	E	Initial	Final
			$\phi=0.2$, time step $\delta t=7\times10^{-6}$ sec					
$X0$	200000	199000	5	0.9098	9.877	5.28	bcc	liquid
Xa	200000	199000	5/2	0.2749	7.544	14.30	$X0$	liquid
Xb	200000	199000	5/4	0.1216	6.048	31.82	Xa	liquid
Xc	249000	199000	5/8	0.0722	5.140	55.88	Xb	liquid
Xd	200000	199000	5/16	0.0530	4.620	77.71	Xc	liquid
Xe	200000	199000	5/32	0.0446	4.336	94.49	Xd	liquid
Xf	200000	199000	5/64	0.0407	4.187	104.96	Xe	liquid
Xg	200000	199000	5/124	0.0388	4.110	110.89	Xf	liquid
Xh	200000	199000	5/256	0.0378	4.071	114.18	Xg	liquid
Xi	200000	199000	5/512	0.0374	4.052	119.67	Xh	bcc
Xj	200000	199000	5/1024	0.0372	4.042	117.85	Xi	bcc
Xk	219300	199000	0	0.0369	4.032	118.67	Xj	bcc
Xl	200000	199000	0	0.0369	4.032	118.45	bcc	bcc
Xm	200000	199000	0	0.0369	4.032	110.74	bcc	bcc
			$\phi=0.3$, time step $\delta t=3\times10^{-6}$ sec					
$G0$	350000	399000	5	0.5055	10.570	8.56	bcc	liquid
Ga	399000	399000	5/2	0.1796	8.073	21.37	$G0$	liquid
Gb	350000	399000	5/4	0.0876	6.472	44.22	Ga	liquid
Gc	350000	399000	5/8	0.0550	5.500	73.20	Gb	liquid
Gd	350000	399000	5/16	0.0416	4.943	100.66	Gc	liquid
Ge	437230	399000	5/32	0.0356	4.639	119.18	Gd	liquid
Gf	350000	399000	5/64	0.0327	4.480	131.25	Ge	liquid
Gg	350000	798000	5/128	0.0313	4.398	137.92	Gf	glass
Gh	542150	399000	5/256	0.0307	4.356	141.41	Gg	glass
Gi	350000	399000	5/512	0.0303	4.335	143.14	Gh	glass
Gj	350000	399000	5/1024	0.0302	4.325	144.12	Gi	glass
Gk	359600	399000	0	0.0300	4.314	145.12	Gj	glass

final state Xk of our slow-quench simulation is a compositionally disordered bcc, similar to Xl. We believe that this is a limitation due to finite size and finite time of our simulation and probably also due to a high energy barrier; otherwise the system would have reached its proper equilibrium state given by run Xm.

III. RESULTS

A. Mean-squared displacement

We have calculated the total mean-squared displacement defined by

$$\langle\langle[\Delta\vec{r}(t)]^2\rangle_N\rangle_{N_c}=\frac{1}{N_c}\sum_{t_0=1}^{N_c}\left[\frac{1}{N}\sum_{i=1}^{N}\{\vec{r}_i(t+t_0)-\vec{r}_i(t_0)\}^2\right] \tag{5}$$

and also the partial MSD $\langle\langle[\Delta\vec{r}_\alpha(t)]^2\rangle_{N_\alpha}\rangle_{N_c}$ for both types of particles ($\alpha=1$ or 2), defined similarly as in Eq. (5), where $\vec{r}_i(t)$ is the position of the particle i at time t. The signal-to-noise ratio of the MSD is increased by averaging over a set of typically $N_c=50$ initial conditions $\{t_0\}$ chosen at different times in the same run. These initial configurations were separated in time $\geqslant\tau_d$ ($\sim10^{-3}$ sec). In liquid state τ_d is the time taken for a particle to diffuse an interparticle separation a_s. The time-dependent diffusion constant and its asymptotic value are given by [24]

$$D(t)=\frac{1}{6t}\langle\langle[\Delta\vec{r}(t)]^2\rangle_N\rangle_{N_c} \tag{6}$$

and

$$D^\infty=\lim_{t\to\infty}D(t). \tag{7}$$

The partial $D_\alpha(t)$ and D_α^∞ are defined similarly. The temporal evolutions of the partial MSD are shown in Figs. 1–4 in log-log plots for various temperatures while cooling the system towards a crystal for $\phi=0.2$ and a glass for $\phi=0.3$. The corresponding results for partial $D(t)$ are given in Figs. 5–8, also in log-log plots. The time dependences of the partial MSD for the small as well as the large particles are similar. The total MSD and the total $D(t)$ show the time dependences which are concentration weighted average of the partial ones and hence are not shown here.

The power-law dependence of MSD [or $D(t)$] can be expressed as $\langle\langle[\Delta\vec{r}(t)]^2\rangle_N\rangle_{N_c}\propto t^m$ [or $D(t)\propto t^{m-1}$], where the exponent m is 1 for Fickian diffusion and less than 1 for

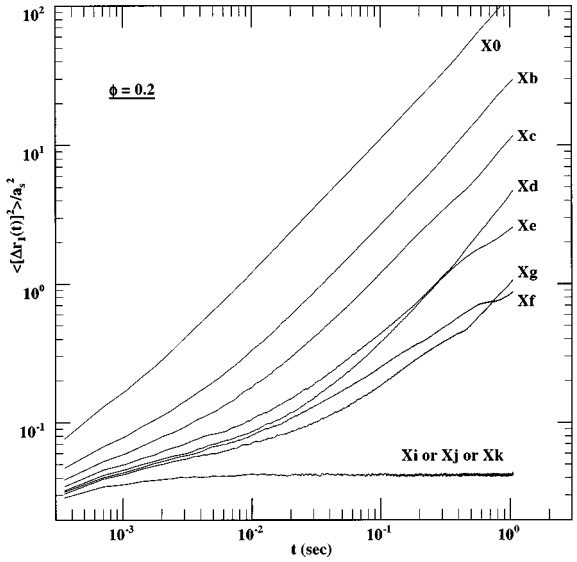

FIG. 1. The lighter sublattice mean-squared displacements $\langle\langle[\Delta\vec{r}_1(t)]^2\rangle_{N_1}\rangle_{N_c}/a_s^2$ versus time (in sec) in a log-log plot for $\phi=0.2$ runs listed in Table I.

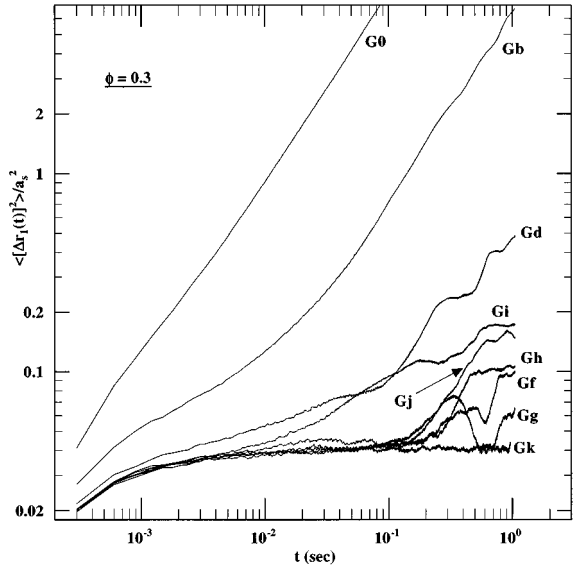

FIG. 3. The log-log plot of $\langle\langle[\Delta\vec{r}_1(t)]^2\rangle_{N_1}\rangle_{N_c}/a_s^2$ versus time (in sec) for $\phi=0.3$ runs listed in Table I.

subdiffusion. The log-log plot is a convenient way to present the data since a MSD with a power-law dependence should show up as a straight line with slope m in this plot and hence the distinction between the diffusive and the subdiffusive regimes should be quite apparent [20,25]. Figure 9 shows the local slope parameter m as a function of time for (a) $\phi=0.2$ and (b) $\phi=0.3$, as obtained from the total MSD. The curves are smoothened using a wavelet filtering technique [26]. There are considerable fluctuations in the value of m close to zero. The long-time values of m (Fig. 9) indicate that the dynamics is considerably diffusive ($m\approx1$) at high temperatures, whereas the particles are localized or trapped ($m\approx0$) in crystal (run Xk) or glassy states (run Gk) at the lowest temperatures. At high and intermediate temperatures ($T^\star>0.0530$ for $\phi=0.2$ and $T^\star>0.0550$ for $\phi=0.3$ in Table I), the general nature of MSD (Figs. 1–4) and $D(t)$ (Figs. 5–8) follow three distinct stages. The initial stage can be associated with the cage diffusion and has $m\approx1$. The choice of δt does not allow us to follow this regime for over a sufficient time in our simulations. Following this, there is an intermediate ''subdiffusive'' regime ($m<1$) and a long-time diffusive behavior ($m\approx1$). Figures 1–4 clearly show that the linear temporal dependence of MSD and hence approximating the long-time diffusion constant from the asymptotic slope of MSD is valid for runs $X0$–Xc with $\phi=0.2$ and runs $G0$–Gb with $\phi=0.3$. As the temperature is lowered more than that corresponding to the above runs, the span of the subdiffusive regime increases successively to cover the entire simulation time, so that the asymptotic values of the diffusion constants are not reached. We note that the short-

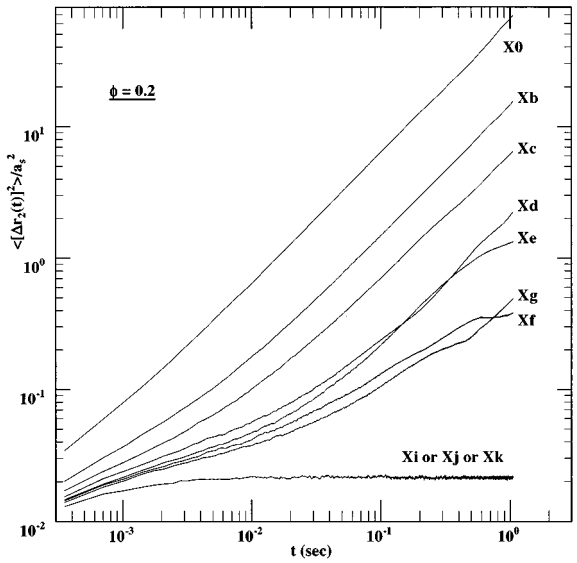

FIG. 2. Same as in Fig. 1, but for the heavier sublattice $\langle\langle\Delta\vec{r}_2(t)]^2\rangle_{N_2}\rangle_{N_c}/a_s^2$.

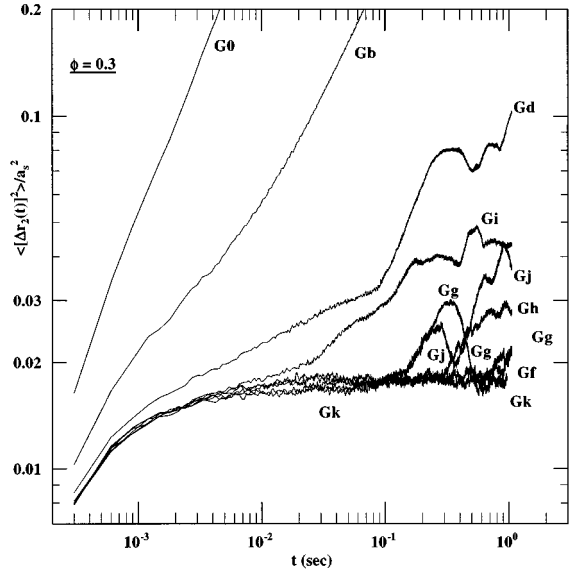

FIG. 4. The log-log plot of $\langle\langle[\Delta\vec{r}_2(t)]^2\rangle_{N_2}\rangle_{N_c}/a_s^2$ versus time (in sec) for $\phi=0.3$ runs listed in Table I.

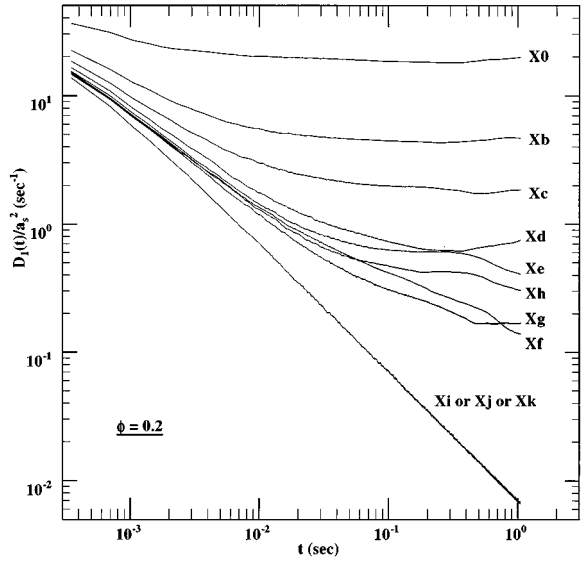

FIG. 5. The lighter particle $D_1(t)/a_s^2$ (in sec^{-1}) versus time (in sec) in a log-log plot for $\phi=0.2$ corresponding to the MSD data shown in Fig. 1.

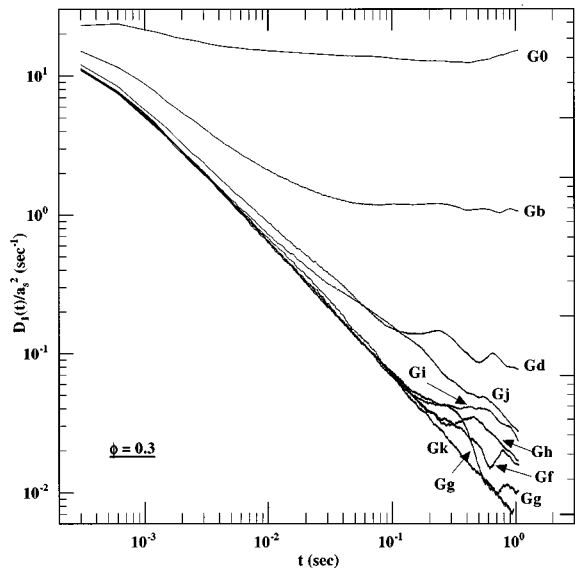

FIG. 7. Same as in Fig. 5, but for $\phi=0.3$.

time profiles of the MSD due to a cage diffusion followed by a subdiffusion are very similar to those obtained in a recent experiment [27] and simulation [28]. The subdiffusive behavior has been very recently calculated theoretically [29] and has been noted in the MD simulations of one-component and binary r^{-12} soft-sphere systems [30,31], monodisperse Yukawa fluid [24,32], LJ systems [33], and also in the nearest-neighbor-interacting lattice gas [34]. It has been suggested that the motion of a particle in the background of an inhomogeneous medium may lead to the subdiffusion.

An immediate distinction between the nature of MSD's, whether a liquid is cooled towards a crystalline or a glassy state (as apparent from the curves below *Xc* in Figs. 1 and 2 and below *Gb* in Figs. 3 and 4) is that the MSD's in the $\phi=0.3$ case alone show a ''staircase'' behavior [which appears as humps in the corresponding $D(t)$ curves]. This indicates that in the supercooled liquid or glassy regime, a particle, in its course of movement, repeatedly gets arrested for a period of time in a ''cage'' formed by its neighbors and subsequently hops to other cages. The fact that the steplike behavior is seen in the statistically averaged quantity MSD points out that the hoppings from one cage to another are taking place cooperatively. The underlying dynamics become extremely slow as shown by the small MSD at these low temperature states and thus the various initial configurations involved in the averaging of MSD are not independent of each other. Hence cooperative hops of the order of an interparticle separation a_s by a few particles will show up as steps in these plots even after averaging over the particle numbers as well as the configurations. The staircase behavior is seen even after averaging of MSD over 100 initial con-

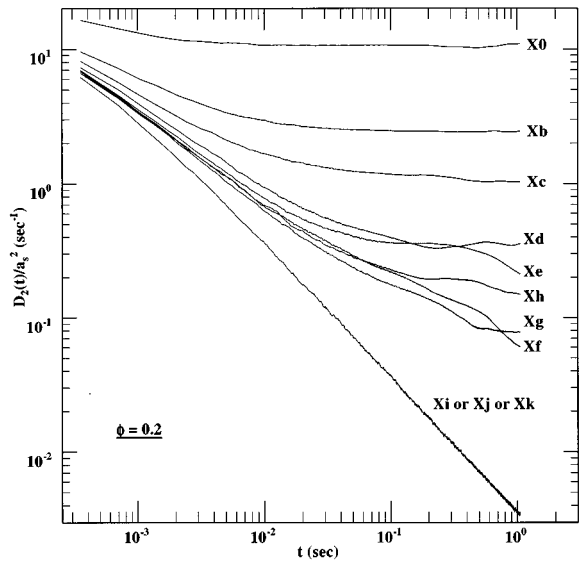

FIG. 6. The heavier particle $D_2(t)/a_s^2$ (in sec^{-1}) versus time (in sec) in a log-log plot for $\phi=0.2$ corresponding to the MSD data shown in Fig. 2.

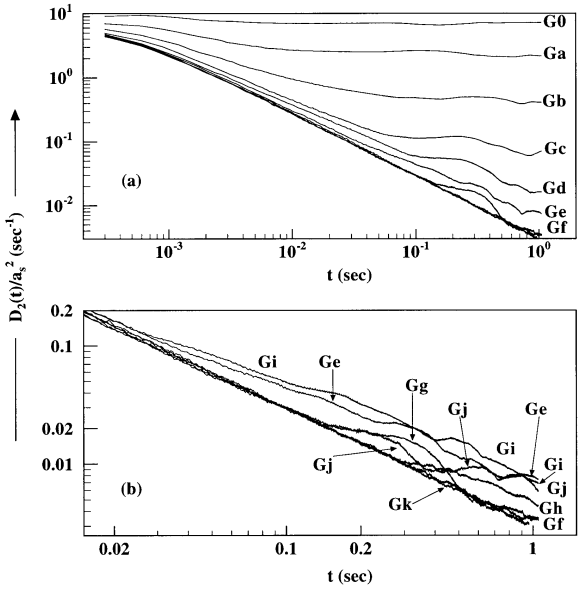

FIG. 8. Same as in Fig. 6, but for $\phi=0.3$. The data are shown in two panels for clarity.

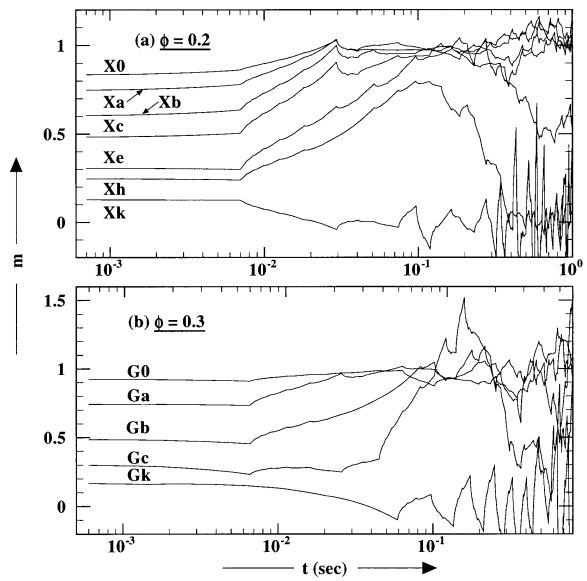

FIG. 9. The temporal dependence of the local slope parameter m is shown in semilogarithmic plots for (a) $\phi=0.2$ and (b) $\phi=0.3$, obtained from the total $\langle\langle[\Delta\vec{r}(t)]^2\rangle_N\rangle_{N_c}/a_s^2$ in those states.

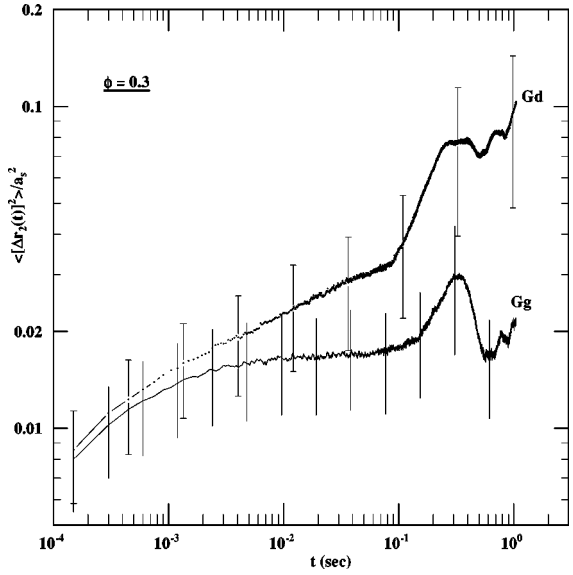

FIG. 10. The MSD $\langle\langle[\Delta\vec{r}_2(t)]^2\rangle_{N_2}\rangle_{N_c}/a_s^2$ for heavier sublattice versus time (in sec) in a log-log plot for the run Gd ($T^\star=0.0416$) and run Gg ($T^\star=0.0313$) at $\phi=0.3$. The error bars represent the average deviation of the individual particle MSD from the corresponding partial MSD.

figurations in the state Gg which has been run for twice the time steps as compared to others (see Table I). We do realize that this averaging over initial configuration may not be sufficient. If we perform averaging over totally independently prepared initial conditions (which will be prohibitively expensive because the state at a given temperature is prepared by successive cooling and equilibration as shown in Table I), it is very likely that the steps can be smoothened out. We are not in a position to perform such runs. (In fact, we are not aware of such computer runs in the available literature on supercooled states). To this end, we have calculated the average deviation $\chi_\alpha(t)$ ($\alpha=1$ or 2) of individual particle MSD's from their corresponding average MSD in the following manner:

$$\chi_\alpha(t)=\langle\langle|\langle[\Delta\vec{r}_\alpha(t)]^2\rangle_{N_\alpha}-[\Delta\vec{r}_\alpha(t)]^2|\rangle_{N_\alpha}\rangle_{N_c}. \qquad (8)$$

In Fig. 10, we have replotted the heavier sublattice MSD for two supercooled liquid states, Gd and Gg, for which the staircase behavior is seen in Figs. 3 and 4. The average deviation $\chi_2(t)$ is reported in Fig. 10 as error bars at several different times (equally separated on logarithmic scale). For both of these cases averaging is performed over a set of N_c different initial configurations chosen in the same run, as explained before. We found that the steps in the MSD are within the limits set by the error bars. The averaging of MSD over several sets of initial configurations separated in time on the same run itself, as explained in Eq. (5), has been widely used in literature for MSD's in liquids as well as in glassy or crystalline states. This procedure works well for liquids (or more generally, for ergodic systems). On the other hand, glass or crystal is a nonergodic system and particles in these states are confined in their positions over a long period of time, practically infinite compared to the total simulation runs achievable with the present day computers and hence do not explore the entire phase space. Even in such cases, this averaging process generates smoother MSD (though not significantly differing from an unaveraged MSD) until a good number of particles execute hopping motion over and above the underlying background of a very slow dynamics, which is clearly the case here. This again suggests that a computationally expensive (and presently intractable) way of averaging over independently prepared sets of initial conditions may be a better averaging procedure for nonergodic systems. On the other hand, it appears that sufficient averaging smears out the interesting aspects of the MSD in the supercooled liquid near the glassy state, distinguishing it from the liquid to crystal transition. Our results suggest that the steps in MSD may be seen in laboratory experiments by digital video imaging of the particles in supercooled binary colloidal mixtures. The cooperative nature of these hops is confirmed by our detailed study of the van Hove self-correlation functions and the individual particle displacements in the vicinity of the glass transition in Secs. III B and III D, respectively. We further note that the reduction in the long-time value of the MSD is sharp for the CT (curves Xh and Xi in Figs. 1 and 2) but gradual for the GT (in Figs. 3 and 4).

The long-time saturation value of the MSD in the crystal (run Xk) and the glass (run Gk) is $\sim 0.04a_s^2$. This gives a value of the Lindemann ratio $W\equiv\sqrt{\langle\langle[\Delta\vec{p}(t)]^2\rangle_N\rangle_{N_c}}$. This can be compared with $W=0.19$ and 0.23 obtained in the MD simulations of Yukawa systems [35] and a monodisperse colloidal suspension with size-corrected DLVO potential [36], respectively, and $W=0.28\pm0.05$ in the Monte Carlo simulation of a polydisperse suspension [37].

In Fig. 11, we have shown the semilogarithmic plots of the asymptotic diffusion constant D^∞ [Eq. (7)] for the CT ($\phi=0.2$), as a function of $1/T^\star$. The values of D^∞ span over more than four orders of magnitude in the range of temperatures shown. The data for the liquid at temperatures above the freezing temperature fit reasonably well to the Arrhenius law (shown by lines in Fig. 11), namely,

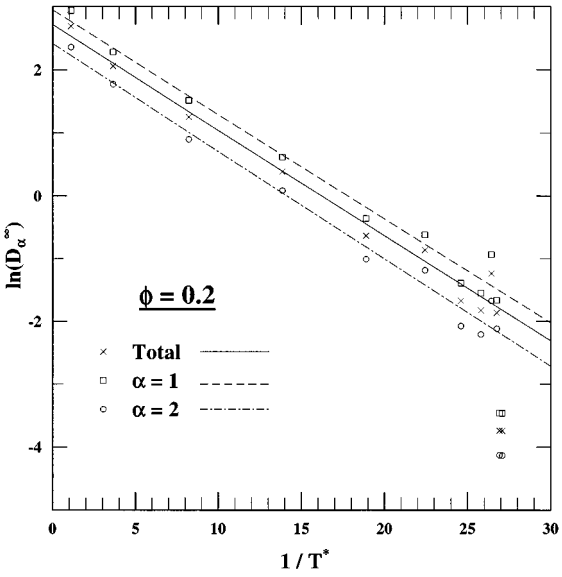

FIG. 11. The natural logarithm of the total D^{∞} and the partial D_{α}^{∞} ($\alpha=1$ or 2) asymptotic diffusion constants (in units of a_s^2/sec) as a function of inverse temperature $1/T^{\star}$ for $\phi=0.2$. The solid lines through the data points are the Arrhenius fits with the fitting parameters given in Table II.

$$D_{\alpha}^{\infty}=A_{\alpha}\exp[(-B_{\alpha}/T^{\star})], \tag{9}$$

with the values of A_{α} and B_{α} given in Table II. The ratio D_1/D_2 fluctuates between 1.7 and 2.1 for the CT data. The Arrhenius temperature dependence of D^{∞} is similar to that of the average relaxation times obtained for the density and the bond-orientational correlation functions of these states [21]. By contrast, the temperature dependence of the average relaxation times in the dense supercooled liquids near the GT is non-Arrhenius [21]. Interestingly, there is an anomalous increase in diffusion at temperatures very near to the CT with respect to its value at the immediate higher temperature. This effect is seen in the MSD and $D(t)$ plots not only for the CT but also for the GT. This is also revealed in Fig. 12, where we plot the value of $\langle\langle[\Delta\vec{r}(t)]^2\rangle_N\rangle_{N_c}/a_s^2$ at $t=1.05$ sec for both the volume fractions. It shows that $\langle\langle[\Delta\vec{r}(t=1.05\ \text{sec})]^2\rangle_N\rangle_{N_c}/a_s^2$ reduces with cooling till some temperature $T_1^{\star}$ and then increases (i.e., the particles are more mobile) till some other temperature $T_2^{\star}<T_1^{\star}$, beyond which it again reduces nearly to zero at the lowest temperature. We call this effect a ''three-stage freezing'' and identify the intermediate state between $T_1^{\star}=0.0407$ (run Xf) and $T_2^{\star}=0.0378$ (run Xh) for the CT and $T_1^{\star}=0.0313$ (run Gg) and $T_2^{\star}=0.0302$ (run Gk) for the GT. The intermediate stage could be the result of a constrained dynamics of more mobile lighter particles in the background of heavier particles and/or a structural readjustment at the onset of a CT or a GT.

TABLE II. The optimal fitting parameters for the Arrhenius law $D_{\alpha}^{\infty}=A_{\alpha}e^{(-B_{\alpha}/T^{\star})}$ for $\phi=0.2$.

Species	A_{α} (in a_s^2/sec)	B_{α}
Total	1.1823	2.7148
$\alpha=1$	1.1801	2.9456
$\alpha=2$	1.1864	2.4153

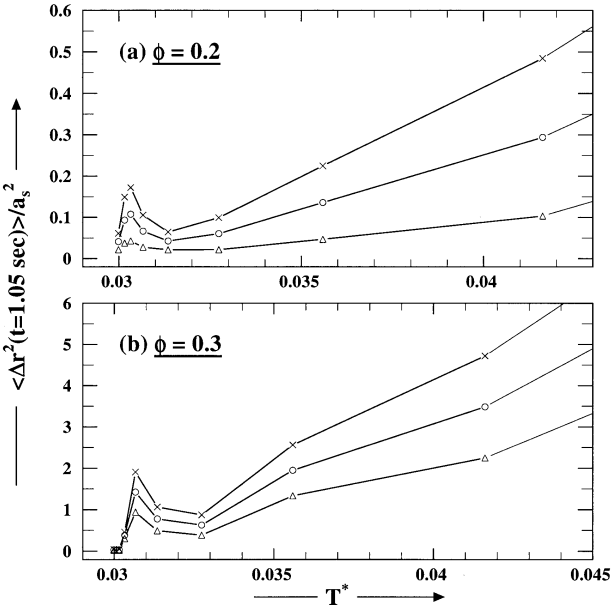

FIG. 12. The total $\langle\langle[\Delta\vec{r}(t=1.05\ \text{sec})]^2\rangle_N\rangle_{N_c}/a_s^2$ (circles) and the partial $\langle\langle[\Delta\vec{r}_{\alpha}(t=1.05\ \text{sec})]^2\rangle_{N_{\alpha}}\rangle_{N_c}/a_s^2$ ($\alpha=1$, crosses; $\alpha=2$, triangles) versus $T^{\star}$ for (a) $\phi=0.2$ and (b) $\phi=0.3$. The data are shown for the eight lowest temperatures in both the cases.

B. van Hove self-correlation function and non-Gaussian parameter

In order to gain a clearer and more quantitative insight into the temporal and spatial dependence of the single-particle motion, we compute the self-part of the van Hove density autocorrelation functions, namely,

$$G_{\alpha}^{s}(r,t)=\frac{1}{N_{\alpha}}\sum_{i=1}^{N_{\alpha}}\langle\delta(|\vec{r}_i^{\alpha}(t)-\vec{r}_i^{\alpha}(0)|-r)\rangle. \tag{10}$$

The angular brackets denote an average over the initial times. The quantity $S_{\alpha}(r,t)=4\pi r^2 G_{\alpha}^{s}(r,t)$ gives the probability that a particle of type α, which was at the origin at time $t=0$, has moved a distance r in time t. The δ function is discretized, so that $\delta(r)=1$ for $0<r\leqslant\Delta r$ and $\delta(r)=0$, otherwise. The choice of the bin width Δr does not affect the results except for the obvious smoothing at large values of Δr. The value of Δr in our simulation is chosen to be one-thousandth of the box length. The function $S_{\alpha}(r,t)$ is normalized such that $\int_0^{\infty}S_{\alpha}(r,t)dr=1$. This function has been extensively studied in the simulations for charge-polydisperse colloidal suspensions [10], r^{-12} soft-sphere alloys [17], LJ mixtures [16], molten salt [38], methanol [39], etc.

The ''Gaussian approximation'' to $G_{\alpha}^{s}(r,t)$ is given by [40,41]

$$G_{\alpha}^{s}(r,t)=\frac{1}{(4\pi D_{\alpha}^{\infty}t)^{3/2}}\exp\left(-\frac{r^2}{4D_{\alpha}^{\infty}t}\right), \tag{11}$$

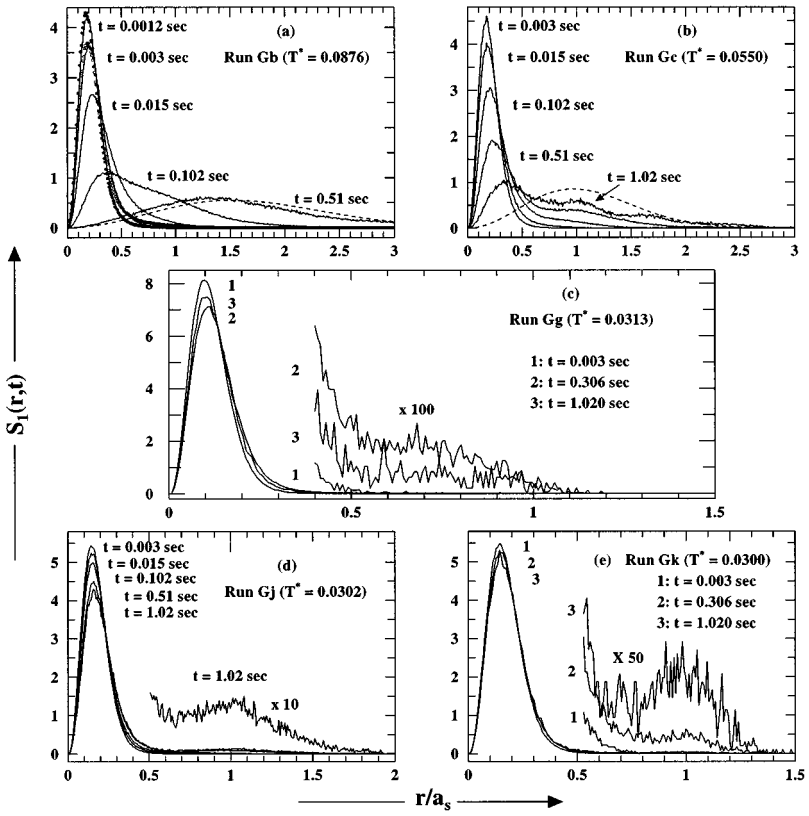

FIG. 13. The van Hove self-correlation functions for the lighter particles at five different temperatures [(a)–(e)] and at a few different times for each temperature for the glass transition ($\phi = 0.3$). In (a) and (b) the dashed line represents the hydrodynamic limit.

which is the Green function for the diffusion equation in three dimensions [41],

$$\frac{\delta G_\alpha^s(r,t)}{\delta t} = D_\alpha^\infty \nabla^2 G_\alpha^s(r,t), \tag{12}$$

subject to the boundary condition $G_\alpha^s(r,0)=\delta(r)$. When the particles execute discrete hops, Eq. (11) is satisfied only for times much larger than the hopping time. The validity of Eq. (11) can be simply tested by calculating the moments [40]

$$\langle |\vec{r}_i^{\,\alpha}(t) - \vec{r}_i^{\,\alpha}(0)|^n \rangle_{t_0} \equiv \int r^n G_\alpha(r,t) dr, \tag{13}$$

where the angular brackets indicate an average over all the particles of type α and the set of initial times $\{t_0\}$. The MSD of a particle of type α after a time t is given by the second moment [i.e., $n=2$ in Eq. (13)] of $G_\alpha^s(\vec{r},t)$. The Gaussian approximation implies, for example, that the non-Gaussian parameter, defined by

$$a_\alpha(t) = \frac{3\langle |\vec{r}_i^{\,\alpha}(t) - \vec{r}_i^{\,\alpha}(0)|^4 \rangle}{5\langle |\vec{r}_i^{\,\alpha}(t) - \vec{r}_i^{\,\alpha}(0)|^2 \rangle^2} - 1, \tag{14}$$

would be identically equal to zero.

The location $r_\alpha^{\max}$ of the maximum of $S_\alpha(r,t)$ indicates the most probable position of the particle at time t, given that it was at the origin at $t=0$. In the hydrodynamic limit, $(r_\alpha^{\max})^2 = 4D_\alpha^\infty t$. The approach to the hydrodynamic limit slows down with decreasing temperature. In a solid (glass or crystal), $r_\alpha^{\max}$ stabilizes after a short while to a time-independent finite value $r_\alpha^{\max} = \sqrt{\langle u_\alpha^2 \rangle}$ where u_α is the thermal displacement of a particle of type α from its mean equilibrium position.

1. Behavior of $S_\alpha(r,t)$

A few representative plots of $S_\alpha(r,t)$ in the supercooled liquid for the lighter particles are given in Fig. 13 for $\phi=0.3$ and Fig. 14 for $\phi=0.2$. To reveal the characteristic diffusive motion, we have shown $S_\alpha(r,t)$ at several different times for a few temperatures. The high temperature liquidlike behaviors are similar for both the volume fractions, a typical example of which is shown in Fig. 13(a), for the run Gb. The function has a single peak, whose position $r_\alpha^{\max}$ moves rapidly to larger r with time t and reasonably reproduces the long-time hydrodynamic limit of Eq. (11), shown by the dashed line in Fig. 13(a). For temperatures close to the supercooled liquid or glass [Figs. 13(d) and 13(e)], $r_\alpha^{\max}$ become nearly independent of time, implying that the system is kinetically frozen. The area under the first peak reduces gradually to give rise to a second peak at the interparticle spacing $r=a_s$, whose height increases with time, as can be seen from the magnified curves, in Figs. 13(d) and 13(e). The increment of the second peak at the cost of the first, even at the lowest temperature case for $\phi=0.3$, is a clear manifestation of the slow relaxation of the quenched disordered states via activated jump processes. We reiterate that these must be taking place cooperatively to get reflected in the statistically average quantities like MSD and $S_\alpha(r,t)$. For a slightly supercooled liquid [e.g., the run Gc in Fig. 13(b)], the dynamics at earlier times is essentially similar to that seen in Fig. 13(a), except for the fact that the overall motion has slowed down so that the hydrodynamic limit (shown by the dashed

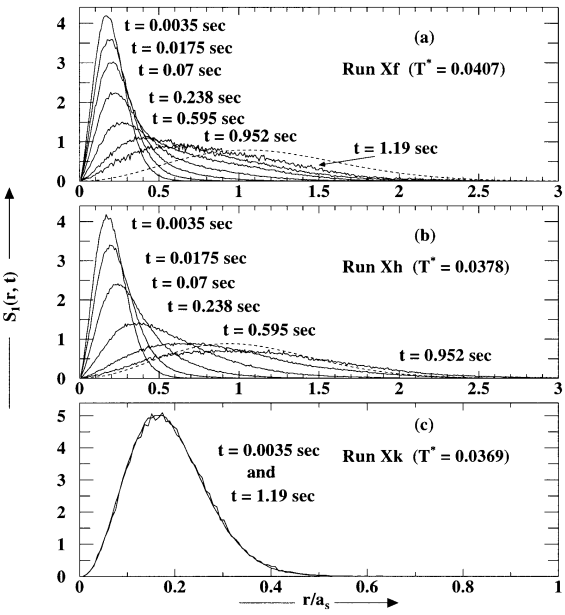

FIG. 14. The van Hove self-correlation functions for the lighter particles at three different temperatures [(a)–(c)] and at a few different times for each temperature for the crystal transition ($\phi = 0.2$). In (a) and (b) the dashed line represents the hydrodynamic limit.

line) is not accessible even in the total simulation time (~ 1.2 sec). The increment of a third peak is also apparent in the data for $t = 1.02$ sec. The crossover of the qualitative nature of the single-particle motion, from diffusive to hop dominated, allows a clear-cut estimation of the crossover temperature $T_c^\star = 0.0356$ (run Ge). This is slightly higher than the estimated $T_c^\star = 0.0325$ from the mode-coupling theory fits of the nonergodicity parameters [42]. This slight ($\sim 9\%$) discrepancy is probably due to the fact that the van Hove self-correlation functions do not take into account all the decay channels and hence are expected to overestimate the transition temperature $T_c^\star$. In the long-time hydrodynamic limit [Eq. (11)], $S_\alpha(r,t)$ scales with $D_\alpha^\infty t$. In Fig. 13(a), we have compared the $S_1(r, t = 0.003$ sec) (full circles) and $S_1(r, t = 0.015$ sec) (open circles) of the run Gc, both scaled by D_1^∞, with $S_1(r, t = 0.0012$ sec) and $S_1(r, t = 0.003$ sec), respectively, for the run Gb (solid lines), showing that this scaling property is valid far before the hydrodynamic limit is reached [17].

The situation for the case of CT is quite different at lower temperatures. There is no indication of the growth of a second or a third peak at a_s or $2a_s$, respectively, demonstrating that the hopping events are almost absent. This is confirmed by the direct observation of the particle displacements, presented in Sec. III D. At the lowest temperature [run Xk in Fig. 14(c)], the system is kinetically arrested over the entire simulation time, as can be seen from complete overlap of the curves calculated for the times $t = 0.0035$ and 1.19 sec.

There are two anomalous features to be noted [25]. (i) Figure 13(c) shows an increase of the first peak height at a later time ($t = 1.02$ sec) (at the cost of the second peak), after the conventional decrease at somewhat earlier time ($t = 0.306$ sec). This clearly indicates that some particles must be hopping back very much cooperatively to their original positions, as confirmed in Sec. III D. (ii) A comparison between the first-peak heights at later times in panels (c) and (d) of Fig. 13 and also in panels (a) and (b) of Fig. 14 shows unambiguously that the system at a certain low temperature (run Gj for $\phi = 0.3$ and run Xh for $\phi = 0.2$) is less rigid than at a slightly higher temperature (run Gg for $\phi = 0.3$ and run Xf for $\phi = 0.2$). This is a manifestation of the three-stage freezing, noted earlier in this paper. A detailed analysis of the microscopic single-particle motion in a latter subsection has led us to the qualitative understanding of how it has taken place prior to both the GT and the CT.

In Figs. 15(a) and 15(b), $(r_\alpha^{\max})^2$ is shown for the lighter and heavier species, respectively, as a function of temperature for various times. Since the identification of a peak in $S_\alpha(r,t)$ is difficult at long times for higher temperatures, this quantity is extracted only at the intermediate and low temperatures. We have checked that at $T^\star > 0.0530$ for $\phi = 0.2$ and $T^\star > 0.0550$ for $\phi = 0.3$, the results approximately follow the expected $(r_\alpha^{\max})^2 = 4D_\alpha t$ behavior. The results seem to indicate that at $T^\star = 0.0307$ (run Gg), the heavier sublattice got completely frozen in the time scale of our simulation. Below this temperature, the problem essentially boils down to that of a constrained dynamics of the lighter particles in the network of the heavier particles.

In the solid phase, $r_\alpha^{\max}$ can be identified with $\sqrt{\langle u_\alpha^2 \rangle}$ (defined before) and hence the ''Lindemann ratio'' $L_\alpha = \sqrt{\langle u_\alpha^2 \rangle}/d_\alpha$ can be determined. Here d_α denotes the mean interparticle spacing for the species α and can be taken as the first peak position of the corresponding partial PDF, $g_{\alpha\alpha}(r)$. Table III gives the values of L_α ($\alpha = 1,2$) for the states Gj and Gk with $\phi = 0.3$ and Xk with $\phi = 0.2$. As can be seen, the values are lower for the heavier particles. Also, these numbers are comparable for the glass and the crystal.

2. Non-Gaussian parameter $a_\alpha(t)$

Figure 16 shows the non-Gaussian parameter, $a_\alpha(t)$, defined in Eq. (14), as the temperature of the liquid is lowered to obtain either a crystal [panels (a) and (b)] or a glass [panels (c) and (d)]. As stated earlier, after a duration of the order of inverse phonon frequency, this function tends to zero for liquids where the self-diffusion follows the usual Fickian diffusion process. Our results for the highest temperature liquids (shown only for the run $X0$) do show this [30,40,43,44] with a maximum deviation of about 5% for the heavier particles [Fig. 16(b)] and 15% for the lighter ones [Fig. 16(a)]. The system becomes increasingly non-Gaussian in nature as it is cooled down to a state point Xf, and then retrieves the Gaussian character as it is further cooled to crystallize. The parameter $a_\alpha(t)$ for the bcc crystal (run Xk) obtained in our simulation shows a deviation of about 20% from zero for both the species, suggesting its anharmonicity to that extent.

The non-Gaussian parameter quite successfully underlines the importance of the activated processes near the GT [45]. The use of its infinite-time value, satisfying $a_\alpha(t \to \infty) = 0$ for $T > T_g$ while $a_\alpha(t \to \infty) \neq 0$ for $T < T_g$, as a suitable candidate for the order parameter was suggested by Miyagawa and co-workers [44,46]. The maximum of the non-Gaussian parameter is also suggested to be a useful parameter to define the glass transition point in a recent trapping diffusion theory [45]. Our BD results on $a_\alpha(t)$ for the GT, as presented in

Figs. 16(c) and 16(d), are interesting. The maximum value of $a_\alpha(t)$ increases dramatically with cooling down to the state point Ge and then decreases till the state point Gg, after which it again increases in the state Gj. Compared to those for $\phi=0.2$ in panels (a) and (b), the maxima in $a_\alpha(t)$ in panels (c) and (d) are unusually high before the glass transition has taken place, implying a significant enhancement of the activated mechanisms (such as correlated jumps) in liquids near the glassy regime. A quantitative comparison of the peak height of $a_\alpha(t)$ shows that the systems investigated here in the states near the GT are much more non-Gaussian than those reported in earlier simulations [30,40,43,44]. In the run Gg, $a_\alpha(t)$ clearly feature the cooperative to and fro hop motions associated with both the species in the time interval between 0.2 and 0.5 sec and also the cooperative hops mostly of the lighter particles (type 1) for $t \geq 0.7$ sec. These motions will be much more clearly revealed from our analysis of tagged-particle motion in Sec. III D. Figures 16(c) and 16(d) also indicate that the heavier sublattice has formed a glass at this temperature but not the lighter ones, as noted earlier in this paper.

C. van Hove distinct-correlation function

In order to study the collective dynamics of the system, we have investigated the temporal evolution of the distinct part of the van Hove density autocorrelation function:

$$G^d_{\alpha\beta}(r,t)=\frac{1}{\sqrt{N_\alpha N_\beta}}\sum_{i=1}^{N_\alpha}\sum_{j=1}^{N_\beta}{}' \langle \delta(\vec{r}-\vec{r}_i^{\alpha}(0)+\vec{r}_j^{\beta}(t))\rangle. \tag{15}$$

The prime on the summation indicates $j\neq i$. $G^d_{\alpha\beta}(r,t)$ specifies the probability distribution to find a particle at a distance r from the origin after a time t, provided another particle was at the origin at $t=0$. At $t=0$, $G^d_{\alpha\beta}(r,t)$ is identically equal to its static counterpart $g_{\alpha\beta}(r)$. In a liquid $G^d_{\alpha\beta}(r,t)$ relaxes rapidly and reaches a value 1 at long times. As the temperature is lowered towards the GT this rapid decay slows down and ''frozen-in'' structure persists even at extremely long times. In Figs. 17(a)–17(d), we have shown $G^d_{\alpha\alpha}(r,t)$ at four different temperatures and at each temperature for various times to picture the collective dynamics near the GT in the system with $\phi=0.3$. The initial static structure is almost completely relaxed by about $t=0.816$ sec for the state point Gb in panel (a), in contrast to the state point Gk in panel (d) where the final glassy structure is attained as early as $t=0.003$ sec. For the run Gd [Figs. 18(a) and 18(b)], after an initial rapid decay corresponding to the vibration in a cage and the β relaxation steps in its corresponding density correlation function $F^s_\alpha(q,t)$ [23] in q space, $G^d_{\alpha\beta}(r,t)$ stabilizes during 0.05 sec $\leqslant t \leqslant$ 0.3 sec corresponding to the plateau in $F^s_\alpha(q,t)$. Beyond this time, a much slower third-stage relaxation implying the beginning of α relaxation is also apparent in Fig. 18(b).

As we have seen above, the difference of the plateau value of $G^d_{\alpha\beta}(r,t)$ from the initial $g_{\alpha\beta}(r)$ is a combination of a fast relaxation and β relaxation. We also note that this difference is discernible primarily in the first neighbor shell ($r/a_s<1.2$) as seen in Fig. 18 and in other $G^d_{\alpha\beta}(r,t)$ [23].

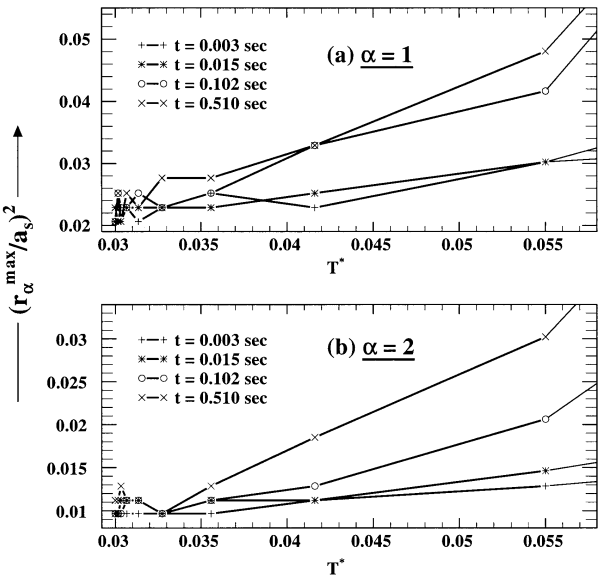

FIG. 15. The square of the location of the first maximum $r_\alpha^{\max}$ (in units of a_s) of $G^s_\alpha(r,t)$ is shown at several different times and different temperatures for the case of glass transition ($\phi=0.3$). (a) The lighter ($\alpha=1$) and (b) the heavier ($\alpha=2$) particles.

This clearly supports the picture that β relaxation is a localized process involving only a few nearest neighbors [47].

We have studied the decay of $G^d_{\alpha\beta}(r,t)$ to its plateau value in the run Gd [Figs. 18(a) and 18(b) for $G^d_{11}(r,t)$] by monitoring the difference $[G^d_{\alpha\beta}(r,t)-G^d_{\alpha\beta}(r,t=0.3\ \text{sec})]$ as a function of t. This quantity indeed follows a factorization of the type predicted by the mode-coupling theory in the β relaxation regime, namely,

$$[G^d(r,t)-G^d(r,t=0.3\ \text{sec})]=H(r)[f(t)-f(0.3\ \text{sec})], \tag{16}$$

where we have dropped the pair indices $\alpha\beta$. The function $H(r)$ is shown in Fig. 19 for various times. One can note small differences in $H(r)$ corresponding to different times below $r/a_s<0.5$.

D. Investigation on tagged-particle motion

In a dense supercooled liquid or an amorphous solid, apart from the vibrational motion around the local potential minimum position, the particles can execute jump motion between the neighboring equilibrium positions. It is easier to trace out such motions in a supercooled liquid near GT, because, in general, the particles are much more localized compared to that in a liquid. In this subsection, we characterize

TABLE III. The Lindemann ratio $L_\alpha=\langle u^2_\alpha\rangle^{1/2}/d_\alpha$ for the species α in the glassy ($\phi=0.3$) and the crystalline ($\phi=0.2$) states.

State	Run	$T^\star$	L_1	L_2
Glass	Gj	0.0302	0.1608	0.1067
	Gk	0.0300	0.1378	0.0933
Crystal	*Xk*	0.0369	0.1684	0.0933

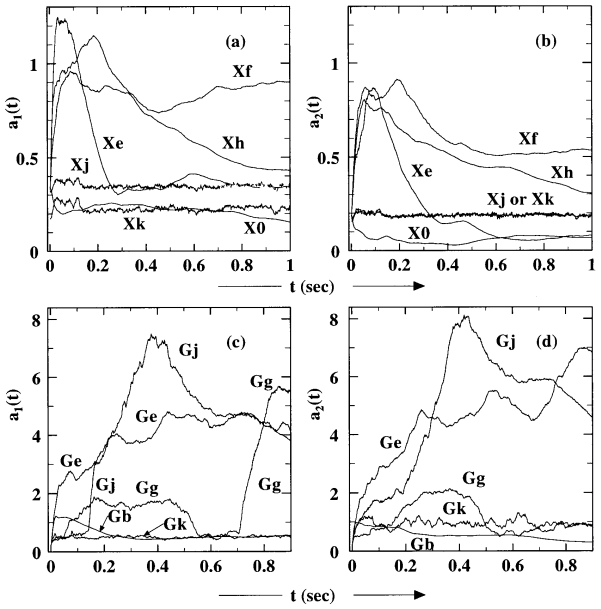

FIG. 16. The non-Gaussian parameter $a_\alpha(t)$ ($\alpha=1$ and 2) at different temperatures. (a) and (b): $\phi=0.2$; (c) and (d): $\phi=0.3$.

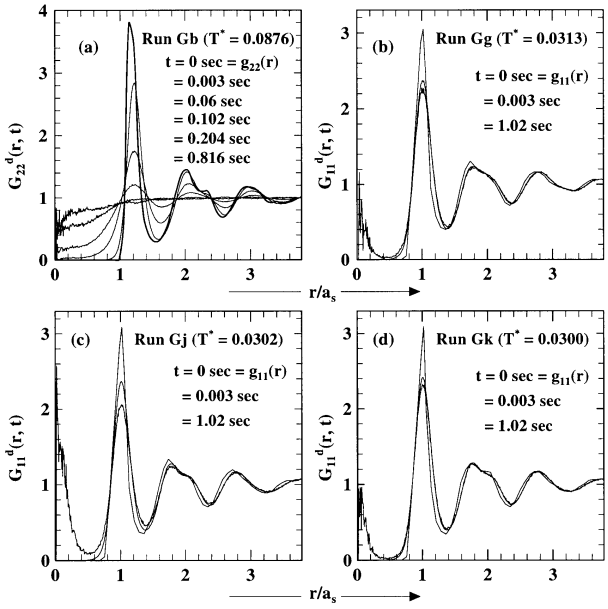

FIG. 17. $G_{\alpha\beta}^d(r,t)$ versus r/a_s for four different temperature runs in (a)–(d) at $\phi=0.3$. The time t from the top to bottom in each panel corresponds to the curves with decreasing height of the primary maximum.

the single-particle motion at the state points Gg, Gj, and Gk for $\phi=0.3$ and Xf and Xh for $\phi=0.2$. This study is motivated by the following facts. First, for the supercooled liquid close to GT, the presence of a staircase profile in its MSD at long times and a second peak in $G_\alpha^s(r,t)$ indicate the breakdown of usual Fickian diffusion implying that the hop motion must be prevailing in these states. Since both of these quantities are statistically averaged, these directly point out towards the cooperativeness of the hop motion. Interestingly, in the run Gg (see Fig. 22), these quantities indicate that quite a few particles have simultaneously hopped by about an interparticle separation a_s, stayed in the new position for a very long time compared to the time of vibration in a cage, and then have hopped back cooperatively to their respective original positions. Second, the unusually high value of a_α near the GT indicates that a cause for the higher mobility of the particles at lower temperatures (three-stage freezing) could be due to an increasing number of hopping events taking place starting from the temperature at which the heavier sublattice freezes first. Finally, the presence of hop and hop-back events in the tagged-particle motion at temperatures near $T_g^\star$ for different systems can specify some sort of a universality in the occurrence of such a behavior very close to the GT.

In order to quantify the tagged-particle motion, we have studied the displacement of each particle over the entire simulation run with respect to its initial position, i.e.,

$$\delta r_i(t) \equiv |\vec{r}_i(t) - \vec{r}_i(0)|. \tag{17}$$

If the particle i, after executing local vibrations up to some time $t=t_1$ makes a jump of the order of a_s, then $\delta r_i(t)$ would remain small ($\sim 0.1a_s$) for $t<t_1$ and at $t\geq t_1$ would suddenly increase to a value $\sim a_s$, thereby clearly distinguishing the jump-type motion. To have a precise idea about the direction of these jumps, one requires use of the other two polar coordinates, namely, $\delta\theta_i(t)$ and $\delta\phi_i(t)$.

In Table IV, we have accumulated the number of particles having their maximum displacement $\delta r_i^{\max} \equiv \max[\delta r_i(t)]$ over the entire period of simulation into three categories, namely, I: $\delta r_i^{\max} < 0.75a_s$, II: $0.75a_s \leq \delta r_i^{\max} \leq a_s$, and III: $\delta r_i^{\max} > a_s$. The particles belonging to classes II and III contribute mainly to the diffusion while those in class I contribute to the average properties of the system.

1. Supercooled liquid ($\phi=0.2$)

Table IV shows that there are 373 particles in class III for the run Xh ($T^\star=0.0378$) making this state point more liquidlike compared to a higher temperature run Xf ($T^\star=0.0407$) where the number of class III particles are only 261. This suggests that significant configurational readjustment has taken place in the run Xh (for which $T^\star \simeq T_f^\star$) to favor the crystallization. The results for the time dependence of the displacements $\delta r_i(t)$ of a few representative particles for runs Xf and Xh are shown in Figs. 20 and 21, respectively. The curves from top to bottom represent $\delta r_i(t)$ of the particles in order of decreasing $\delta r_i^{\max}$ and they are shifted by some multiple of a_s from each other for clarity. The panels marked 2 are the results for the heavier (type 2) particles and the rest are for the lighter ones. These figures do show the presence of a very few jump events, which were not discernible in the corresponding van Hove self-correlation functions. The jumps are ''smoother'' (i.e., the flight time is much more than the typical vibrational period) in run Xh than in run Xf. When compared to Figs. 22–24, we see that the particle motion before the CT is much smoother and hence diffusive than the relatively hindered hop-trap motion of the particles in the GT case (which we discuss in the next paragraph).

2. Supercooled liquid-glass ($\phi=0.3$)

Figures 22, 23, and 24 present $\delta r_i(t)$ for the runs Gg, Gj, and Gk, respectively. We clearly see that four types of par-

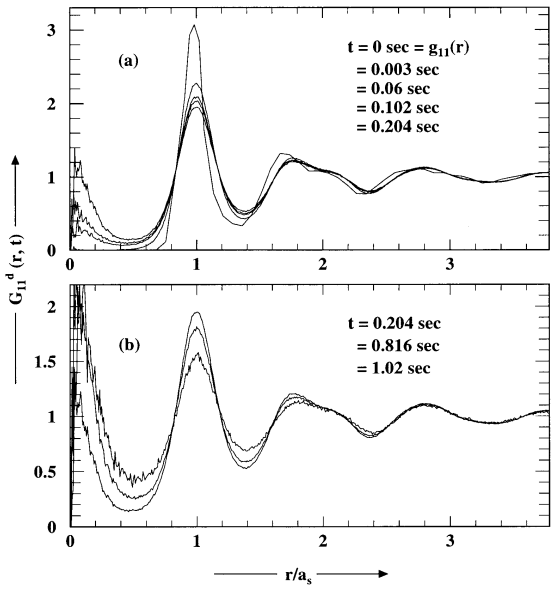

FIG. 18. $G^{d}_{\alpha\beta}(r,t)$ versus r/a_s for the run Gd ($T^{\star}=0.0416$) at $\phi=0.3$. The time t from the top to bottom in (a) and (b) corresponds to the curves with decreasing height of the primary maximum.

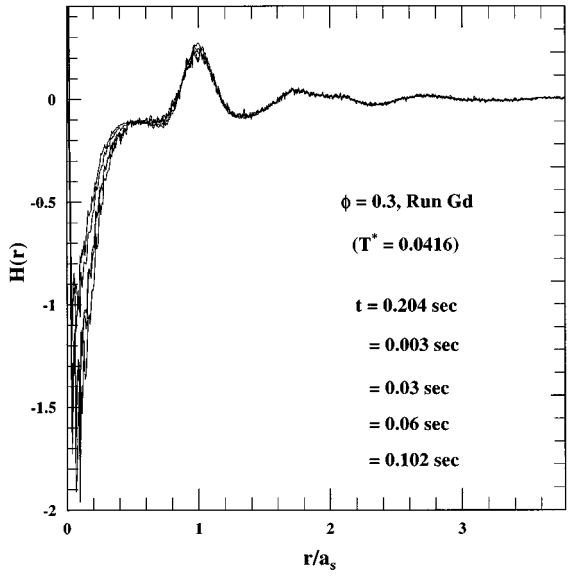

FIG. 19. The function $H(r)$ for the run Gd ($T^{\star}=0.0416$) at $\phi=0.3$. The curves from the top to bottom are for $t=0.204$, 0.003, 0.03, 0.06, and 0.102 sec.

ticle motions are present, namely, (A) vibrations around the local potential minimum, (B) hopping of the order of a_s to a neighboring equilibrium position and persisting there till the end of the simulation run, (C) transient vibrations, i.e., hopping by $\sim a_s$ to a new position, staying there for a short while [to a maximum of ten times the time scale of motion (A)] and then hopping back to its original position and (D) motion similar to (C) but time of residence in the hopped position being quite high [more than 100 times the time scale of (A)]. In the glassy state (run Gk, Fig. 24), the hop-back motion of type (D) is altogether absent, and the transient vibrations (C) are not very frequent, showing that the majority of particles perform small amplitude vibrational motion. This is also indicated by the fact that about 95% of the particles belong to class I in Table IV. For the runs Gg (Fig. 22) and Gj (Fig. 23), all the four types of motion are very frequent. A comparison of the numbers of class III particles between these two states from Table IV may not reflect the higher mobility in the lower temperature state point Gj, but a closer look into the single-particle dynamics shows that in the run Gj, there are ten particles which moved $\geqslant 1.4a_s$ contributing largely to the diffusion, compared to only five of them in Gg. Most jumps in the run Gg are sharp, with the flight time being less than 0.003 sec. This is in contrast to the case in run Gj, where the flight times are typically much more than 0.003 sec and thereby contributing towards an increased diffusion or the three-stage freezing. Though there are a few particles at this temperature executing jumps and occasionally jump-back motions almost together, a careful comparison shows that the overall cooperativeness in particle motion is much less than that seen in the run Gg. Any fluctuation of one particle in Gg is very strongly correlated with a few other particles and hence show up in the statistically averaged quantities too. The reasons for which the run Gg has been continued for double the time compared to the other runs in the series (refer to Table I) are at least twofold, first, to show that the jump-type motions are very frequent and their cooperativeness indeed is a property of the system at this temperature and secondly, to improve upon the statistics for the calculations of the MSD and van Hove functions. We note that even at this temperature, where most of the particles are localized to their respective local equilibrium positions, a few of them have executed jump motion of type (D) cooperatively at the similar times. In particular, we have followed the movement of seven particles, which simultaneously executed hop movements with $0.90a_s<\delta r_i^{\max}<1.15a_s$ at $t\approx 0.3$ sec and after persisting in the new position for up to $t\approx 0.48$ sec, have hopped back to their respective initial positions. This has been done to check if they permute their positions to show a rotation or caterpillar motion which is different than hole-induced jumps. These sorts of particle motion near the GT have been identified in earlier MD simulations of soft-sphere binary mixtures interacting via r^{-12} potential [46,16]. We have named these particles A–G, in descending magnitude of their maximum movement in the total duration of the run Gg (Fig. 22). The averaging of coordinates is performed over all the BD steps as follows: (i) before the hop, between $t=0$ and $t=0.24$ sec; (ii) at the hopped position, between $t=0.3$ sec and $t=0.48$ sec; and (iii) after the return, between $t=0.54$ sec and $t=0.66$ sec. The averaged coordinates thus available for these seven particles at times (i) and (iii) overlap almost identically and hence when plotted in Fig. 25, we can often see only two points corresponding to the initial (marked A–E) and the hopped positions (marked A'–E'). By calculating the interparticle distances among these particles in their initial and hopped positions, we have categorized them into three groups: (1) $E\rightleftharpoons G$, (2) $A\rightleftharpoons D\rightleftharpoons B\rightleftharpoons C$, and (3) F. From Figs. 22 and 25, we see that at around $t=0.3$ sec, in group (1), the particle G hops to some position G', leaving a vacancy behind where E hops in. During the same time, in group (2), A hops to D, D to B, and B to C in a sequential chainlike motion. The group (3) particle F makes a hop to a neighbor-

TABLE IV. The number of particles with maximum displacements $\delta r_i^{\max}$ in different spatial intervals defined by I: $\delta r_i^{\max} < 0.75a_s$; II: $0.75a_s \leq \delta r_i^{\max} \leq a_s$; III: $\delta r_i^{\max} > a_s$. The displacements are measured with respect to the location of the particles at the beginning of the corresponding simulation run.

State	Run	$T^\star$	I	II	III
Glass	Gg	0.0313	373	30	29
	Gj	0.0302	385	23	24
	Gk	0.0300	408	12	12
Crystal	Xf	0.0407	83	88	261
	Xh	0.0378	13	46	373

ing position F' during this time. These particles stay at their hopped position between $t=0.3$ sec and 0.48 sec. Beyond this time, surprisingly enough, they almost simultaneously hop back to their respective original positions and persist there. As stated earlier in this paper, the flight time of these hop or hop-back motions are ~ 0.003 sec and the residence time ~ 0.2 sec. The initial state and the configuration after the cooperative and interconnected hop can perhaps be viewed as two states of the ''two-level'' system conjectured to occur in the glassy regime.

We have noted above that the cooperative hop-back motion is present for at least two different runs with temperature very close to $T_g^\star$ and $\phi=0.3$. In Fig. 26, we present the results of a similar analysis of $\delta r_i(t)$ on a system with similar parameters but with $N=256$ particles. An initial bcc lattice is melted with $n_i=5n_p\overline{Z}$ and the resultant liquid configuration is further cooled to $n_i=0.1n_p\overline{Z}$ in one step. The effective temperature of the system is $T^\star=0.0360$ which is

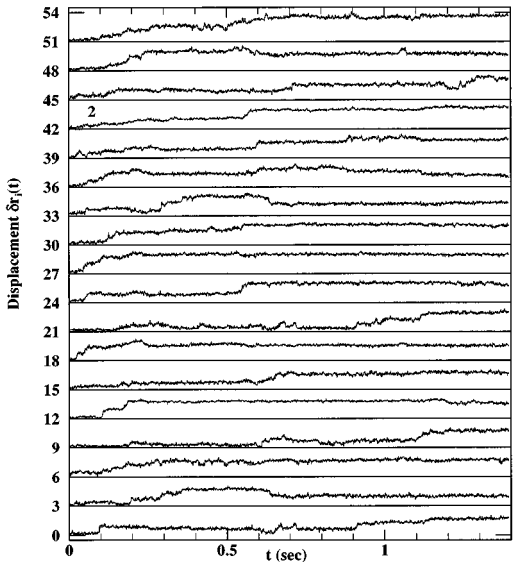

FIG. 20. The function $\delta r_i(t)$ (in units of a_s) from the top to bottom for a few representative particles in the run Xf ($\phi=0.2$, $T^\star=0.0407$) in order of decreasing $\delta r_i^{\max}$. The curves are shifted vertically by some multiples of a_s from each other for the clarity of presentation. The panels marked 2 represent $\delta r_i(t)$ for the heavier particles and the rest are for the lighter particles.

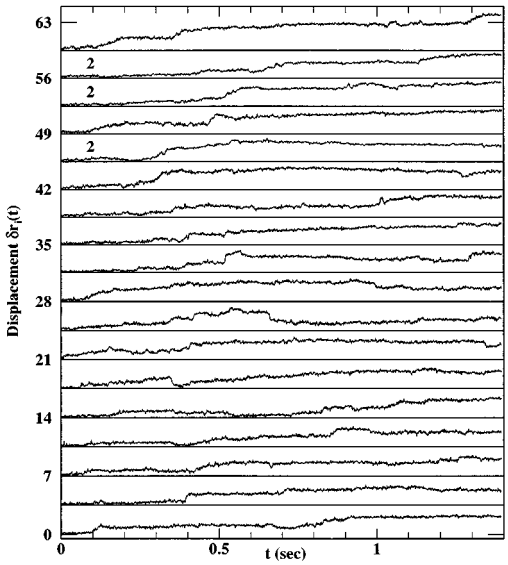

FIG. 21. Same as in Fig. 20, but for the run Xh ($\phi=0.2$, $T^\star=0.0378$).

very close to its GT temperature. The curves $\delta r_i(t)$ in Fig. 26, plotted in a similar manner as before, clearly reveals the presence of strongly cooperative hop and hop-back motion in at least two different time intervals, namely, $t\sim 0.45$ sec to ~ 0.55 sec and $t\sim 1.0$ sec to ~ 1.1 sec. The presence of cooperative hop-back motion for three different phase points close to the GT temperature [namely, the runs Gg ($T^\star=0.0313$) and Gj ($T^\star=0.0302$) for one system and at $T^\star=0.0360$ for an altogether differently prepared system] and also in a recent work [48] support the universality of such an occurrence.

IV. SUMMARY AND CONCLUSIONS

In this paper we have reported the Brownian dynamics simulation results on the dynamical properties for binary po-

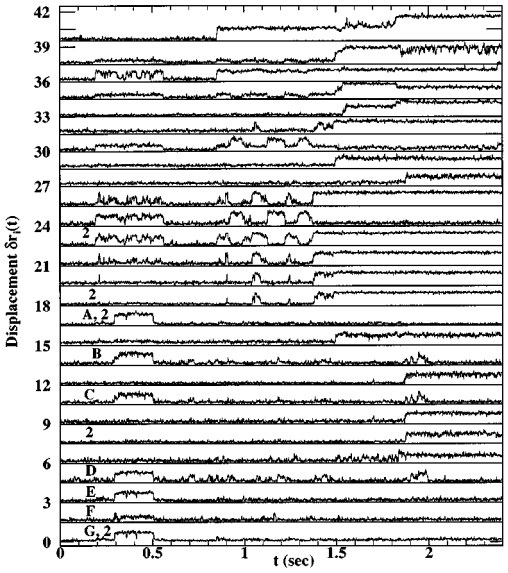

FIG. 22. Same as in Fig. 21, but for the run Gg ($\phi=0.3$, $T^\star=0.0313$). Seven particles executing to and fro hop motions (refer to Fig. 25) are marked A–G.

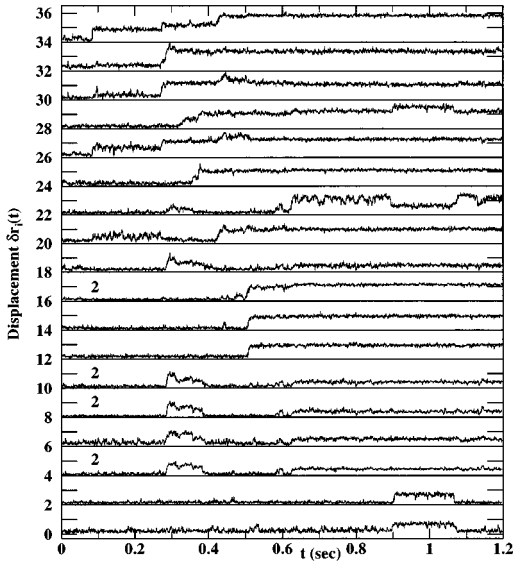

FIG. 23. Same as in Fig. 22, but for the run Gj ($\phi=0.3$, $T^\star=0.0302$).

lyball mixtures interacting via the DLVO potential, as these are cooled towards a crystal or a glass formation. Our main results and conclusions are as follows.

(1) The relaxation scenarios are completely different as a moderately cooled colloidal liquid is further cooled to show a crystal transition for $\phi=0.2$ or a glass transition for $\phi=0.3$. The temporal evolution of the mean-squared displacement shows deviation from the usual Fickian diffusion in the intermediate time scale for $T^\star<0.0530$ for $\phi=0.2$ and $T^\star<0.0550$ for $\phi=0.3$, and follows subdiffusive behavior: MSD $\propto t^m$ with $m<1$. The temporal span of this subdiffusive regime increases with reducing temperature as well as with increasing ϕ. In addition, in the long-time regime, the MSD for the supercooled liquid with $\phi=0.3$ shows a staircase profile indicating strongly cooperative jump motion present in these states.

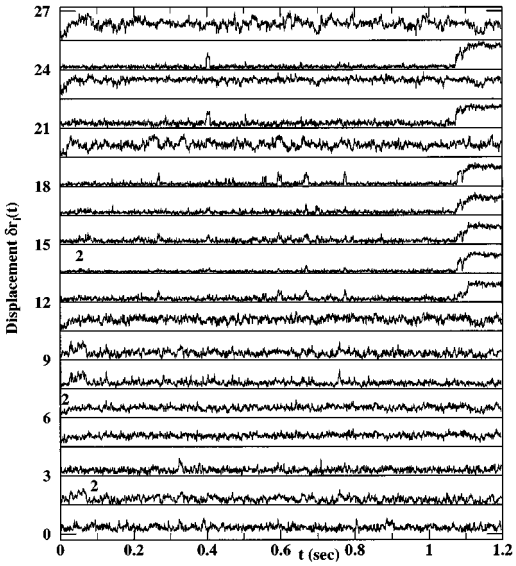

FIG. 24. Same as in Fig. 23, but for the run Gk ($\phi=0.3$, $T^\star=0.0300$).

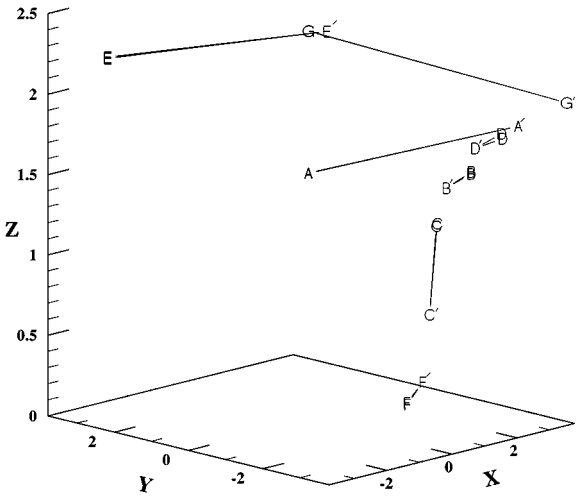

FIG. 25. The averaged coordinates for the seven particles $A-G$ of Fig. 22. Only A and G are heavier particles (type 2). The dimensions of X and Y denote sides of the simulation box in units of a_s.

(2) The shift of $r_\alpha^{\max}$ and the broadening of $G_\alpha^s(r,t)$ with time at high temperatures, to reach the hydrodynamic limit, follow the behavior expected in the liquid states. We have shown that the scaling, given by Eq. (11), starts holding good even at the initial times far before the approach to hydrodynamic limit ($t\to\infty$) for the temperatures where the asymptotic value D_α^∞ is reached. This is in agreement with an earlier work on binary model alloy with r^{-12} pair interaction [17].

(3) As a supercooled liquid is cooled towards the glass transition, a second peak and at times a third peak in $G_\alpha^s(r,t)$ at the first and the second nearest-neighbor positions, respectively, evolve in time, at the expense of the area under the first peak. This clearly shows that the particles execute activated jump motions rendering the system extremely non-Gaussian as characterized in terms of the non-Gaussian parameters $a_\alpha(t)$. The importance of this parameter in quantifying the GT temperature has been stressed in the lit-

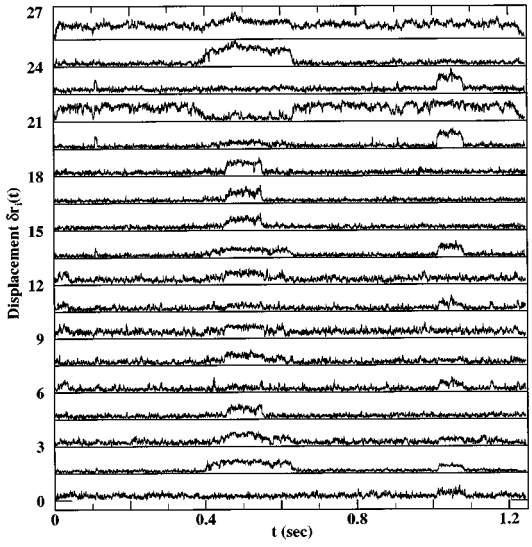

FIG. 26. Same as Fig. 24 but for a state ($\phi=0.3$, $T^\star=0.0360$, $N=256$) arrived at via one-step quench (refer to text).

erature [45]. The strong cooperative behavior of these hop motions near the GT ($\phi=0.3$) makes $a_\alpha(t)$ much larger than that near the crystal transition ($\phi=0.2$), where the hop motions are rare.

(4) The gradual slowing down of the collective dynamics, as probed by $G^d_{\alpha\beta}(r,t)$, shows the presence of two time scales usually associated with the α and β relaxations predicted by the mode-coupling theory for an ideal glass transition. In the β relaxation regime, the difference of $G^d_{\alpha\beta}(r,t)$ from its plateau value obeys a factorization property as per the prediction of the theory.

(5) There exists an intermediate temperature range at which the system is more mobile (liquidlike) than at its immediate higher temperature (three-stage freezing), implying significant structural adjustments. This happens for both $\phi=0.2$ and $\phi=0.3$ and its implications are present in all the dynamical quantities calculated.

(6) A significant result of our simulation is that at a temperature ($T^\star=0.0313$, run Gk) very near to the GT ($T^\star_g=0.0312$), $G^s_\alpha(r,t)$ shows an increase of the first peak height at some later time (at the cost of the second peak). This clearly indicates that a few particles must be hopping back to their original positions from their respective hopped positions. The individual trajectories and displacements of the particles have been followed to find that about 2% of the particles show an interconnected cooperative hop motion with maximum displacements lying between $0.90a_s$ and $1.15a_s$ at $t\sim0.3$ sec, persist at the hopped position for another 0.2 sec, and then again almost simultaneously hop back to their respective initial positions. A maximum of 10% of the particles show marked cooperative hindrance in their motion during this time, such that the effect shows up in the statistically averaged quantities: the MSD, $G^s_\alpha(r,t)$, and $a_\alpha(t)$. This behavior is seen in two more systems very near to the GT. The existence of cooperative hopping motion has been pointed out earlier in the MD simulations of either inverse 12-power binary supercooled liquids near the GT [46,16] or a 6-12 LJ glass [49], but there is no example of the cooperative hop-back motion in literature. To the best of our knowledge, there exists only one experimental evidence [50] of strongly cooperative motion during the structural relaxation of a metallic glass. This was seen by measuring the isotope effect of ^{60}Co diffusion in the $Co_{76.7}Fe_2Nb_{14.3}B_7$ glass, by radiotracer technique. These results indicate the importance of a careful analysis of the glass transition data using the extended version of MCT which incorporates the activated hopping processes [13,14].

ACKNOWLEDGMENTS

We thank the Indo-French Center for the Promotion of Advanced Research (Project No. 607.1) for financial support. We made use of the computational resources of the Jawaharlal Nehru Center for the Advanced Scientific Research, India and the Supercomputer and Educational Research Center of the Indian Institute of Science, India. We thank Professor Jayanth R. Banavar for discussions. S.S. acknowledges helpful discussions with Siddhartha Shankar Ghosh, Jaydeb Chakrabarti, and S. Balasubramanian at various stages of the work.

[1] For a review, see A. K. Sood, in *Solid State Physics*, edited by H. Ehrenreich and D. Turnbull (Academic, New York, 1991), Vol. 45, p. 1.

[2] E. B. Sirota, H. D. Ou-Yang, S. K. Sinha, P. M. Chaikin, J. D. Axe, and Y. Fujii, Phys. Rev. Lett. **62**, 1524 (1989).

[3] P. N. Pusey, W. van Megen, P. Bartlett, B. J. Ackerson, J. G. Rarity, and S. M. Underwood, Phys. Rev. Lett. **63**, 2753 (1989); W. van Megen and P. N. Pusey, Phys. Rev. A **43**, 5429 (1991): W. van Megen, S. M. Underwood, and P. N. Pusey, Phys. Rev. Lett. **67**, 1586 (1991); W. van Megen and S. M. Underwood, Phys. Rev. E **47**, 248 (1993).

[4] P. N. Pusey and W. van Megen, Nature (London) **320**, 340 (1986); Phys. Rev. Lett. **59**, 2083 (1987); S. E. Paulin and B. J. Ackerson, *ibid.* **64**, 2663 (1990); P. N. Pusey, J. Phys. (France) **48**, 709 (1987): W. van Megen and S. M. Underwood, Langmuir **6**, 35 (1990).

[5] S. Yoshimura and S. Hachisu, J. Phys. (Paris), Colloq. **46**, C3-115 (1985); Nature (London) **283**, 188 (1980); P. Bartlett, R. H. Ottewill, and P. N. Pusey, J. Chem. Phys. **93**, 1299 (1990); Phys. Rev. Lett. **68**, 3801 (1992).

[6] S. Yoshimura and S. Hachisu, Prog. Colloid Polym. Sci. **68**, 59 (1983).

[7] H. M. Lindsay and P. M. Chaikin, J. Chem. Phys. **76**, 3774 (1982).

[8] R. Kesavamoorthy, A. K. Sood, B. V. R. Tata, and A. K. Arora, J. Phys. C **21**, 4737 (1988).

[9] A. Meller and J. Stavans, Phys. Rev. Lett. **68**, 3646 (1992); S. Sanyal and A. K. Sood, Pramana, J. Phys. **45**, 1 (1995).

[10] H. Löwen, J. P. Hansen, and J. N. Roux, Phys. Rev. A **44**, 1169 (1991).

[11] For reviews, see W. Götze, in *Liquids, Freezing and the Glass Transition*, Proceedings of the Les Houches Summer School of Theoretical Physics, Session L1, edited by J. P. Hansen, D. Levesque, and J. Zinn-Justin (North-Holland, Amsterdam, 1991), p. 287; W. Götze and L. Sjögren, Rep. Prog. Phys. **55**, 241 (1992).

[12] G. Szamel and H. Löwen, Phys. Rev. A **44**, 8215 (1991).

[13] S. P. Das and G F. Mazenko, Phys. Rev. A **34**, 2265 (1986); W. Götze and L. Sjögren, Z. Phys. B **65**, 415 (1987); J. Phys. C **21**, 3407 (1988); L. Sjögren, Z. Phys. B **79**, 5 (1990); M. Fuchs, W. Götze, S Hildebrand, and A. Latz, J. Phys.: Condens. Matter **4**, 7709 (1992): W. Götze, in *Phase Transitions and Relaxations in Systems with Competing Energy Scales*, Vol. 415 of *NATO Advanced Study Institute, Series C: Mathematical and Physical Sciences*, edited by T. Riste and D. Sherrington (Kluwer Academic, Boston, 1993).

[14] H. Z. Cummins, W. M. Du, M. Fuchs, W. Götze, S. Hildebrand, A. Latz, G. Li, and N. J. Tao, Phys. Rev. E **47**, 4223 (1993).

[15] P. K. Dixon, N. Menon, and S. R. Nagel, Phys. Rev. E **50**, 1717 (1994).

[16] G. Wahsnström, Phys. Rev. A **44**, 3752 (1991).

[17] J. N. Roux, J. L. Barrat, and J. P. Hansen, J. Phys.: Condens. Matter **1**, 7171 (1989).
[18] R. O. Rosenberg, D. Thirumalai, and R. D. Mountain, J. Phys.: Condens. Matter **1**, 2109 (1989).
[19] D. L. Ermak and Y. Yeh, Chem. Phys. Lett. **24**, 243 (1974): D. L. Ermak, J. Chem. Phys. **62**, 4189 (1975): **62**, 4197 (1975): D. L. Ermak and J. A. McCammon, *ibid.* **69**, 1352 (1978).
[20] S. Sanyal and A. K. Sood, Phys. Rev. E **52**, 4154 (1995).
[21] S. Sanyal and A. K. Sood, Phys. Rev. E **52**, 4168 (1995).
[22] M. P. Allen and D. J. Tildesley, *Computer Simulation of Liquids* (Oxford University Press, London, 1987).
[23] S. Sanyal, Ph. D. dissertation, Indian Institute of Science, Bangalore, India, 1994 (unpublished).
[24] K. Kremer, G. S. Grest, and M. O. Robbins, J. Phys. A **20**, L181 (1987).
[25] S. Sanyal and A. K. Sood, Europhys. Lett. **34**, 361 (1996); Prog. Theor. Phys. Suppl. **126**, 163 (1997).
[26] I. Daubechies, *Ten Lectures on Wavelets* (Society of Industrial and Applied Mathematics, Philadelphia, 1992); M. C. Valsakumar (unpublished).
[27] J. Colmenero *et al.*, Phys. Rev. Lett. **71**, 2603 (1993).
[28] R. J. Roe, J. Non-Cryst. Solids **172-174**, 77 (1994); **182**, 329 (1995).
[29] A. V. Indrani and S. Ramaswamy, Phys. Rev. Lett. **73**, 360 (1994).
[30] Y. Hiwatari, B. Bernu, and J. P. Hansen, in *Condensed Matter Theories*, edited by P. Vasishta, Rajiv K. Kalia, and R. F. Bishop (Plenum, New York, 1987), Vol. 2, p. 19.
[31] Y. Hiwatari, J. Phys. Soc. Jpn. **47**, 733 (1979); S. Kambayashi and Y. Hiwatari, *ibid.* **56**, 2788 (1987).
[32] M. O. Robbins, K. Kremer, and G. S. Grest, J. Chem. Phys. **88**, 3286 (1988); M. Wild and R. B. Pandey, Phys. Rev. E **47**, 3246 (1993).
[33] J. Ullo and S. Yip, Chem. Phys. **149**, 221 (1990); F. Ould-Kaddour and J. L. Barrat, Phys. Rev. A **45**, 2308 (1992).
[34] P. Maass, J. Petersen, A. Bunde, W. Dieterich, and H. E. Roman, Phys. Rev. Lett. **66**, 52 (1991); P. Maass, A. Bunde, and M. D. Ingram, *ibid.* **68**, 3064 (1992); R. B. Pandey, Physica A **191**, 438 (1992); **187**, 77 (1992).
[35] K. Kremer, M. O. Robbins, and G. S. Grest, Phys. Rev. Lett. **57**, 2694 (1986).
[36] R. O. Rosenberg and D. Thirumalai, Phys. Rev. A **36**, 5690 (1987).
[37] B. V. R. Tata and A. K. Arora, J. Phys.: Condens. Matter **4**, 7699 (1992).
[38] G. F. Signorini, J. -L. Barrat, and M. L. Klein, J. Chem. Phys. **92**, 1294 (1990).
[39] P. Sindzingre and M. L. Klein, J. Chem. Phys. **96**, 4681 (1992).
[40] A. Rahman, Phys. Rev. A **136**, 405 (1964); J. Chem. Phys. **65**, 4845 (1976); B. R. A. Nijboer and A. Rahman, Physica (Utrecht) **32**, 415 (1966).
[41] J. P. Hansen and I. R. McDonald, *Theory of Simple Liquids*, 2nd ed. (Academic, London, 1986).
[42] S. Sanyal and A. K. Sood (unpublished).
[43] B. Bernu, Y. Hiwatari, and J. P. Hansen, J. Phys. C **18**, L371 (1985); B. Bernu, J. P. Hansen, Y. Hiwatari, and G. Pastore, Phys. Rev. A **36**, 4891 (1987).
[44] H. Miyagawa and Y. Hiwatari, Phys. Rev. A **44**, 8278 (1991).
[45] T. Odagaki and Y. Hiwatari, Phys. Rev. A **41**, 929 (1990); Y. Hiwatari and T. Odagaki, in *Proceedings of the XXIV Yamada Conference on Strongly Coupled Plasma Physics, Lake Yamanaka, Japan*, edited by S. Ichimaru (Elsevier, Amsterdam, 1990), p. 163; T. Odagaki and Y. Hiwatari, J. Non-Cryst. Solids **117/118**, 887 (1990); Phys. Rev. A **43**, 1103 (1991); T. Odagaki, J. Matsui, and Y. Hiwatari, Phys. Rev. E **49**, 3150 (1994), and the references cited therein.
[46] H. Miyagawa, Y. Hiwatari, B. Bernu, and J. P. Hansen, J. Chem. Phys. **88**, 3879 (1988).
[47] M. Goldstein, J. Chem. Phys. **51**, 3728 (1969); G. P. Johari and M. Goldstein, *ibid.* **55**, 4245 (1971).
[48] C. Oligschleger, Solid State Commun. **93**, 1031 (1995).
[49] J. M. Delaye and Y. Limoge, Europhys. Lett. **20**, 421 (1992); J. Phys. I **3**, 2063 (1993): **3**, 2079 (1993).
[50] K. Rätzke, P. W. Hüppe, and F. Faupel, Phys. Rev. Lett. **68**, 2347 (1992).